

Scaling behavior of oscillations arising in delay-coupled optoelectronic oscillators

Lucas Illing,* Greg Hoth, Lauren Shareshian, and Christopher May

Department of Physics, Reed College, Portland, Oregon 97208, USA

(Received 10 November 2010; published 23 February 2011)

We study the effect of asymmetric coupling strengths on the onset of oscillations in delay-coupled nonlinear systems. Our experiment consists of two wide-band optoelectronic devices that are cross-coupled. We find that oscillations appear in the system when the product of the two coupling strengths exceeds a critical value. Beyond the oscillation threshold, the oscillation amplitudes grow smoothly and we find a scaling law that describes the dependence of the amplitude on the coupling strengths. The observations are in good agreement with predictions from linear stability analysis and normal form theory.

DOI: [10.1103/PhysRevE.83.026107](https://doi.org/10.1103/PhysRevE.83.026107)

PACS number(s): 89.75.Da, 42.65.Sf

I. INTRODUCTION

Coupled oscillators have received significant attention over the past decade [1], and a central question is to understand how specific properties of the individual behavior and the coupling architecture can explain the collective dynamics. When oscillators are coupled, non-negligible coupling delays naturally arise because signals in real systems inevitably propagate from one oscillator to the next with a finite propagation speed. These time delays can induce many new phenomena and complex dynamics. This is the case, for example, in neuronal networks [2,3], biological oscillators [4], or coupled optical systems [5–15], and even for a single optical system, the introduction of time-delayed feedback can lead to extremely rich dynamics [16–19].

In this paper, we study instabilities and scaling laws arising in an experimental system consisting of two laser-pumped fiber-coupled Mach-Zehnder modulators (MZM) with a coupling scheme where the output intensity of one MZM is used to modulate the radiofrequency (rf) input of the other MZM. Optical systems with such cross-coupled architecture have received a lot of attention recently because they represent the simplest mutually linked subunit in any larger network [20,21]. A main focus of recent work has been the question of when cross-coupled delay systems exhibit isochronal chaos synchronization under symmetric coupling and operating conditions [15,22,23]. Examples of experimental systems that have been used to study this issue are semiconductor lasers with optical [6,7,14] and optoelectronic [8] coupling, fiber-ring lasers with optical coupling [12,24], MZM nonlinearities with shared feedback [13], and MZM nonlinearities with discrete-time implementation [25]. In addition, scaling laws of periodic oscillations arising under asymmetric coupling conditions have been studied for cross-coupled semiconductor lasers linked optoelectronically [9,10]. In the current paper, we investigate scaling relations for a system with the same cross-coupled architecture as in [9] but with a very different nonlinear device forming each individual oscillator.

The goal of this paper is to present details about our experiment investigating oscillation onsets and scaling under asymmetric coupling conditions, to explain theoretically the observed dependence of the oscillation threshold on the two

coupling strengths, and to shed light on the origin of the observed scaling law, with a focus on separating the role of the coupling architecture and the individual oscillator. We describe the experimental setup and the deterministic device model in Sec. II and present the experimental results in Sec. III. To theoretically explain our results, we perform a linear stability analysis in Sec. IV and use normal form theory to derive a scaling law in Sec. V.

II. EXPERIMENTAL SETUP AND MODEL

In our experiment, schematically shown in Fig. 1(a), continuous-wave light is emitted from two $1.55\ \mu\text{m}$ distributed feedback (DFB) semiconductor lasers. The light from each laser is coupled into a single-mode fiber, passes through a polarization controller, and is injected into a LiNbO_3 MZM. The transmission through the MZM is a nonlinear function of the applied voltage, $P_{\text{out}}/P_{\text{in}} \sim \cos^2(m + \pi V_{\text{rf}}/2V_{\pi,\text{rf}})$, where the applied voltage consists of two components, a time-varying voltage V_{rf} that is ac-coupled into a rf port ($V_{\pi,\text{rf}} = 4.5\ \text{V}$) and a bias voltage applied to a dc-coupled port that sets the phase shift m . In all the experiments discussed in this paper, the MZM was biased to the half-transmission point of the transmission curve ($m = -\pi/4$), as shown in Fig. 1(b). This bias was chosen because under this condition the quiescent state is most linearly unstable.

The optical output of each MZM is routed via two circulators toward the other MZM. For example, light exiting MZM₁ enters port one of circulator C_1 and is routed to port three of circulator C_2 . The optical power in the fibers that couple the two systems is adjusted via variable attenuators. This allows for a separate and repeatable tuning of the two coupling strengths via the attenuator settings, α_{21} (from MZM₁ to MZM₂) and α_{12} (from MZM₂ to MZM₁). The values of α_{12} and α_{21} range between zero and one, denoting, respectively, no transmission and maximum transmission. The optical power is then converted to a voltage by broadband amplified photodetectors (bandwidth 30 kHz–13 GHz).

Half of the resulting signal, denoted by V_1 (V_2) for the left (right) nonlinearity, is measured by a broadband real-time oscilloscope. The other half of the signal is amplified by an inverting modulator driver (gain $g_{\text{MD}} = -23$) and coupled into the rf port of MZM₁ (MZM₂). The modulator drivers saturate for output voltages approaching the saturation voltage $V_{\text{sat}} = 9.7\ \text{V}$. We take this saturation into account by including

*illing@reed.edu

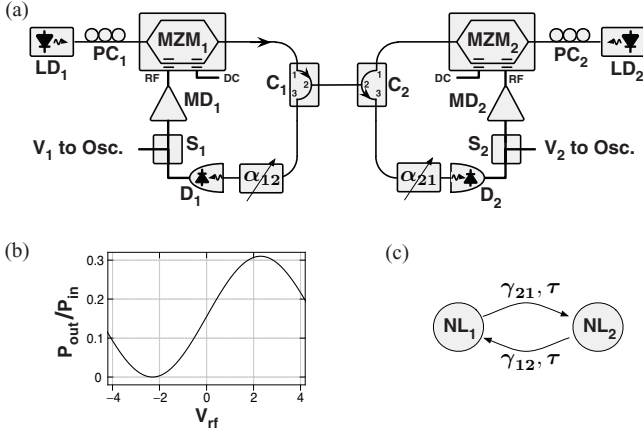


FIG. 1. (a) Schematic of the cross-coupled optoelectronic oscillators: LD, laser diodes; PC, polarization controllers; MZM, Mach-Zehnder modulators; C, optic circulators; α , adjustable optic attenuators; D, photodetectors; S, electronic splitters; MD, modulator drivers. (b) Nonlinear response of the MZM as a function of the rf voltage with the dc voltage such that the MZM is biased at the half-transmission point. (c) Schematic representation of the cross-coupled setup shown in panel (a).

a hyperbolic tangent function in our model of the system nonlinearity,

$$f(x_i) = \cos^2(m + d \tanh x_i) - \cos^2(m), \quad (1)$$

where $d = \pi V_{\text{sat}}/2V_{\pi, \text{rf}}$ is a constant and $x_i = g_{\text{MD}} V_i/V_{\text{sat}}$ ($i = 1, 2$) denotes the dimensionless and scaled variable corresponding to the measured output voltage.

The main contribution to the coupling delays in our system comes from light propagation through lengths of single-mode fiber connecting the various optical components. The two coupling delays are equal. That is, the time it takes signals to propagate from splitter S_1 to splitter S_2 , fixed at $T = 43.9$ ns, is matched to within our measurement uncertainty of 0.1 ns to the time it takes signals to propagate from splitter S_2 to splitter S_1 .

In modeling the dynamics of the optoelectronic oscillators, it is important to take into account that signals are bandpass-filtered [19,26,27]. High frequencies are suppressed due to the finite response time of the system components, and low frequencies are blocked due to the ac coupling of electronic components. For a single MZM with self-feedback, the simplest model describing the linear frequency response with reasonable accuracy is a two-pole bandpass filter, with a high- (low-) frequency cutoff $\omega_+ \approx 7 \times 10^{10} \text{ s}^{-1}$ ($\omega_- \approx 2 \times 10^5 \text{ s}^{-1}$), center frequency $\omega_0 = \sqrt{\omega_+ \omega_-} = 1.2 \times 10^8 \text{ s}^{-1}$, and bandwidth $\Delta \approx \omega_+$. The dynamics of a single MZM with self-feedback is then described by a second-order delay-differential equation (DDE), and previous investigations have shown such a model to be in good agreement with experiments [18,19]. Similarly, two cross-coupled MZM's with delayed coupling are well modeled by a set of coupled dimensionless second-order DDE's,

$$\begin{aligned} \dot{x}_1(s) &= -x_1(s) - y_1(s) + \gamma_{12} f[x_2(s - \tau)], \\ \dot{y}_1(s) &= \epsilon x_1(s), \end{aligned} \quad (2)$$

$$\begin{aligned} \dot{x}_2(s) &= -x_2(s) - y_2(s) + \gamma_{21} f[x_1(s - \tau)], \\ \dot{y}_2(s) &= \epsilon x_2(s). \end{aligned} \quad (3)$$

Here, the overdot denotes the derivative with respect to the dimensionless time $s = t\Delta$, $\tau = T\Delta$ is the coupling delay, $\epsilon = \omega_0^2/\Delta^2$ is a small parameter characterizing the bandpass filter, and f is the nonlinear function given by Eq. (1). The effective coupling strengths γ_{12} and γ_{21} take into account all losses and gains in the system and are directly proportional to α_{12} and α_{21} .

In the experiment and the numerical simulations, all parameters except the coupling strengths are matched and kept fixed ($m = -\pi/4$, $d = 3.4$, $\epsilon = 2.9 \times 10^{-6}$, $\tau = 3073$). When the coupling strengths are increased, bifurcations from steady state all the way to fully developed chaos are observed. In the results reported here, we focus on the first instability, a bifurcation from steady state to periodic oscillations.

III. EXPERIMENTAL RESULTS

The coupling strength α_{12} is increased in experiments for fixed values of the coupling strength α_{21} . For small values of α_{12} , the system exhibits steady-state behavior. The measured nonzero value of the output voltage, $V_1^{\text{rms}} \sim 1$ mV, is mainly due to noise from the photodetector. Beyond a critical value of α_{12} , the steady state becomes unstable, giving rise to periodic oscillations. The amplitude of the initially sinusoidal oscillations grows smoothly as α_{12} is increased, squaring-off and saturating for larger α_{12} . In contrast, the oscillation period remains roughly constant with a value of ~ 22 ns. This is close to one-half of the delay time, $T = 43.9$ ns, implying that the outputs of the two MZM's are in phase and that the signal comes back to itself after completing one round trip (the round-trip delay time is $2T = 87.8$ ns). Thus, small sinusoidal oscillations with this period will be amplified and give rise to the observed stable periodic behavior, if the effective total round-trip gain is larger than 1.

In Fig. 2(a), the oscillation amplitude measured by detector D_1 , that is, V_1^{rms} , is shown as a function of the coupling strength α_{12} for several fixed values of α_{21} . It is seen that the critical value of α_{12} increases as α_{21} decreases. In other words, the system will start to oscillate for weak α_{21} as long as α_{12} is strong enough. Intuitively, one might expect that the critical coupling strength depends on the product $\alpha_{12}\alpha_{21}$ because this product determines the effective round-trip gain. This is confirmed in Fig. 2(b), where we plot the scaled oscillation amplitude versus $\sqrt{\alpha_{12}\alpha_{21}}$ and find that the steady state becomes unstable at a critical constant of $\alpha_c = \sqrt{(\alpha_{12}\alpha_{21})_c} = 0.45$.

From Fig. 2(a) it is also seen that the amplitude growth beyond oscillation onset strongly depends on the fixed value of α_{21} . In Fig. 2(b), it is shown that by plotting the rescaled amplitudes, $V_1^{\text{rms}} \sqrt{\alpha_{21}^2 + \alpha_c^2}$, versus $\sqrt{\alpha_{12}\alpha_{21}}$, all the data collapse onto a single common curve in the region close to the instability threshold. This implies that there exists a single function that determines the oscillation amplitudes for given coupling strengths.

These observations are reproduced in simulations where we numerically integrate the model equations, Eqs. (1)–(3), for various coupling strengths, as shown in Fig. 3. In agreement

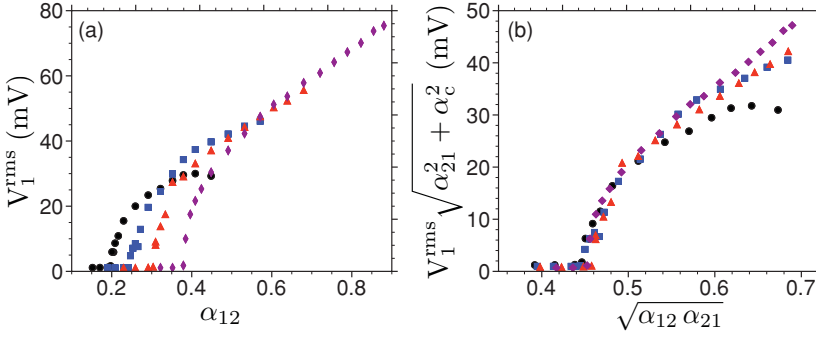


FIG. 2. (Color online) Experimental observations and scaling: (a) Plot of V_1^{rms} , proportional to the intensity oscillation amplitude measured by D_1 , as a function of the coupling strength α_{12} for four different values of α_{21} : $\alpha_{21} = 1$ (black circles), $\alpha_{21} = 0.82$ (blue squares), $\alpha_{21} = 0.69$ (red triangles), and $\alpha_{21} = 0.54$ (purple diamonds). (b) The data collapse when the rescaled oscillation amplitude is plotted vs $\sqrt{\alpha_{12} \alpha_{21}}$.

with the experiment, all data collapse onto a single curve in the vicinity of the instability threshold, when plotting the rescaled amplitude versus $\sqrt{\gamma_{12} \gamma_{21}}$. The critical value of the self-coupling strength of a single MZM nonlinearity with delayed self-feedback is $\gamma_c = 0.294$ for our parameters. It is seen that the instability threshold for a single system is identical to that of a cross-coupled system if one uses $\sqrt{\gamma_{12} \gamma_{21}}$ as the bifurcation parameter.

IV. LINEAR STABILITY ANALYSIS

In this section, we use linear stability analysis of the steady-state solution to determine the oscillation threshold. Since the results of linear stability analysis do not depend on the detailed properties of the nonlinear device used, we perform the analysis in a more general setting by considering an arbitrary network of identical delay-coupled single-input–single-output systems under the assumption that the tunable parameters that lead to a bifurcation are the coupling strengths (including self-feedback) and that all delays are identical. In this general setting, we show how the oscillation threshold of the network can be understood in terms of the coupling architecture and the oscillation threshold of a single oscillator. Applied to the particular case of the experiment, this analysis shows that the square root of the product of the two coupling strengths is the relevant bifurcation parameter for a cross-coupled system, and that the threshold is identical to that of a single system with self-feedback.

A. Single system with self-feedback

To relate the network behavior to properties of an individual oscillator, we first examine a single system with delayed self-feedback. To be specific, consider a single-input–single-output system with scalar input u and scalar output y . The output is taken to be some function of the state variables, $y = h(\mathbf{x})$. The input is $u = \gamma y^\tau$ for a single system with delayed self-feedback, where $y^\tau = y(t - \tau)$ denotes the delayed output variable and γ is the strength of the tunable self-coupling. The DDE describing the dynamics of a single system is then

$$\dot{\mathbf{x}} = \mathbf{F}(\mathbf{x}) + \gamma \mathbf{b} h(\mathbf{x}^\tau), \quad (4)$$

where $\mathbf{x} \in \mathbb{R}^m$, $\mathbf{b} \in \mathbb{R}^m$ is an input vector, and \mathbf{F} is a vectorial function describing the internal dynamics. It is assumed that coordinates are chosen such that $h(0) = \mathbf{F}(0) = 0$ and therefore $\mathbf{x} = 0$ is a steady-state solution. The local stability

of this steady-state solution is determined by investigating the linearized equation [28],

$$\dot{\mathbf{x}} = D\mathbf{F} \mathbf{x} + \gamma D\mathbf{H} \mathbf{x}^\tau. \quad (5)$$

The output is given by $y = \mathbf{c}\mathbf{x}$ with $\mathbf{c} = (dh/dx_1, \dots, dh/dx_m)$, $D\mathbf{H} \in \mathbb{R}^{m \times m}$ is defined by $D\mathbf{H} = \mathbf{b}\mathbf{c}$, $D\mathbf{F} \in \mathbb{R}^{m \times m}$ denotes the Jacobian matrix of \mathbf{F} , and all derivatives are evaluated at $\mathbf{x} = 0$. Using, in Eq. (5), the solution ansatz $c_\lambda \exp(\lambda t)$ for a nonzero m -vector c_λ , one obtains the corresponding characteristic equation, the solutions of which are the characteristic values λ . We assume that for sufficiently small self-coupling strength γ , there are no characteristic values with a positive real part and that, as γ is increased, the steady state loses stability at $\gamma = \gamma_c$ through an Andronov-Hopf bifurcation, which means that there is a pair of simple characteristic values $\lambda(\gamma) = \alpha(\gamma) \pm i\omega(\gamma)$ crossing transversally the imaginary axis at $\gamma = \gamma_c$ [$\alpha(\gamma_c) = 0, \omega(\gamma_c) = \Omega > 0, \alpha'(\gamma_c) > 0$] and there are no other characteristic values with zero real parts [29]. In Appendix A, we show that Andronov-Hopf bifurcations are generically expected for single-input–single-output systems with long delay and input-output transfer functions with bandpass characteristics.

B. Delay-coupled network

A network of N identical systems coupled to one another with strength γ_{ij} and identical coupling delay τ is modeled by a set of coupled DDE's,

$$\dot{\mathbf{x}}_i = \mathbf{F}(\mathbf{x}_i) + \sum_{j=1}^N \gamma_{ij} \mathbf{b} h(\mathbf{x}_j^\tau), \quad i = 1, \dots, N \quad (6)$$

with steady-state solution $\mathbf{X} = 0$, where \mathbf{X} is an $(m \cdot N)$ column vector, $\mathbf{X} = (\mathbf{x}_1, \mathbf{x}_2, \dots, \mathbf{x}_N)^\top$. Linearizing Eq. (6) yields

$$\dot{\mathbf{X}} = [\mathbb{1}_N \otimes D\mathbf{F}] \mathbf{X} + [\Gamma \otimes D\mathbf{H}] \mathbf{X}^\tau, \quad (7)$$

where \otimes is the Kronecker product, $\mathbb{1}_N$ is the N -dimensional identity matrix, and Γ is the $N \times N$ coupling matrix with elements γ_{ij} . Focusing on the case where Γ is diagonalizable, let σ_i (\mathbf{v}_i) be the set of eigenvalues (eigenvectors) of the coupling matrix Γ , such that $\Gamma \mathbf{v}_i = \sigma_i \mathbf{v}_i$. Writing \mathbf{X} in terms of the network eigenvectors as $\mathbf{X} = \sum_{i=1}^N \mathbf{v}_i \otimes \mathbf{u}_i(t)$, where the $\mathbf{u}_i(t)$ are m -dimensional column vectors, Eq. (7) simplifies to a set of N uncoupled DDE's,

$$\dot{\mathbf{u}}_i = D\mathbf{F} \mathbf{u}_i + \sigma_i D\mathbf{H} \mathbf{u}_i^\tau, \quad i = 1, \dots, N, \quad (8)$$

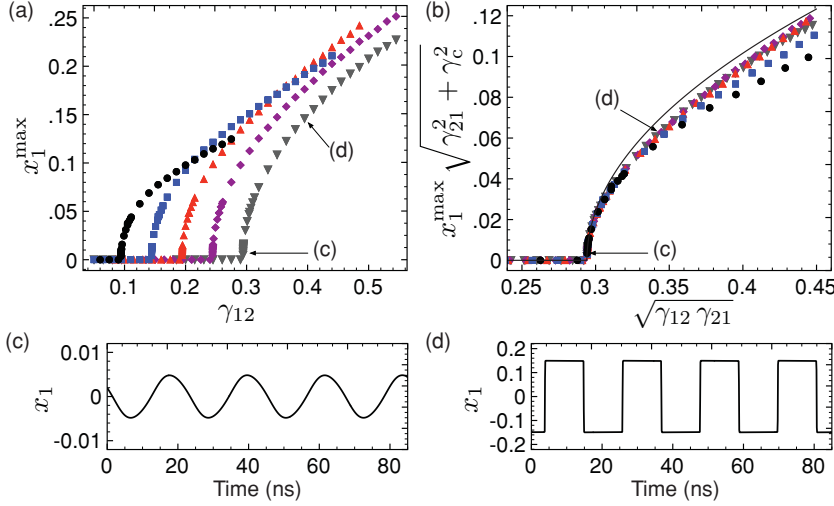


FIG. 3. (Color online) Numeric results: (a) Amplitude for oscillations with period $\sim \tau/2$ as a function of the coupling strength γ_{12} for five different values of γ_{21} : $\gamma_{21} = 0.92$ (black circles), $\gamma_{21} = 0.6$ (blue squares), $\gamma_{21} = 0.45$ (red up-triangles), $\gamma_{21} = 0.35$ (purple diamonds), and $\gamma_{21} = 0.29$ (gray down-triangles). (b) The data collapse when the rescaled oscillation amplitude is plotted vs $\sqrt{\gamma_{12}\gamma_{21}}$. The solid black line shows the analytically derived result (see Sec. V). (c) and (d) Two examples of $x_1(t)$ corresponding to coupling parameters indicated in panel (a) and (b).

one for each eigenvalue σ_i . Equation (8) is seen to be identical to Eq. (5), except that σ_i can be complex-valued, in contrast to γ , which is real. Nevertheless, the problem is now separated into a part that deals exclusively with the topology of the network and a part that only depends on the dynamics of a single system. One may thus first find, for a single system, regions of steady-state stability in the complex σ plane. Then the steady-state solution is stable for a given network of N systems, if all N eigenvalues σ_i are located inside stability regions.

For the particular case of two cross-coupled optoelectronic oscillators, Eqs. (2) and (3), the two coupling-matrix eigenvalues are $\sigma_1 = \sqrt{\gamma_{12}\gamma_{21}}$ and $\sigma_2 = -\sqrt{\gamma_{12}\gamma_{21}}$, corresponding to in-phase and antiphase oscillations, respectively. From these eigenvalues it is immediately clear that the instability threshold depends on the product of the coupling strength, in agreement with experiments. Investigating the stability region of a single oscillator (see Appendix), we find the stability region in the σ plane to be a nearly perfect circle of radius $|\sigma_c| = \gamma_c = 1/d \simeq 0.29$ with corrections on the order of 10^{-7} . Taking these higher-order corrections into account [see Eq. (20) in [26]], it can be shown that in theory σ_1 crosses the stability boundary before σ_2 as γ_{12} is increased. However, given the limitations of actual experiments, this distinction is meaningless because in this case even a small deviation of the experimental transfer function from the ideal behavior can have noticeable effects. That is, if the transfer function has a gain that is slightly higher for some particular frequency than theoretically assumed by the two-pole bandpass-filter approximation, then the mode closest to this frequency will be preferred. Indeed, in our experiment we find that the frequency of the observed in-phase mode coincides with a small local peak (<3 dB) in the transfer function.

The fact that the stability boundary is a circle with radius γ_c in the complex σ parameter plane is not specific to the optoelectronic oscillator but holds to a good approximation for any single-input-single-output systems with long delay and bandpass characteristics (see Appendix). Thus, for a network of N such systems, the steady state is stable if all network eigenvalues satisfy $|\sigma_i| < \gamma_c$, and an Andronov-Hopf bifurcation occurs, generically, if the eigenvalue with the

largest magnitude crosses this boundary as the connection strengths γ_{ij} are varied.

It is often useful to have an equation determining the bifurcation threshold in terms of the experimentally controllable connection strengths. One can obtain such an equation without having to solve for the entire spectrum of eigenvalues σ_i in cases in which it is known, *a priori*, that the eigenvalue of Γ with the largest magnitude is positive and real. In that case, the equation

$$\det(\Gamma - \gamma_c \mathbb{1}_N) = 0 \quad (9)$$

relates the γ_{ij} to the known critical self-coupling strength of a single system (γ_c). As an example, two cross-coupled systems with self-feedback reach the bifurcation threshold when the four coupling strengths satisfy

$$\gamma_c^2 + \gamma_{11}\gamma_{22} - \gamma_c(\gamma_{11} + \gamma_{22}) - \gamma_{12}\gamma_{21} = 0. \quad (10)$$

One condition that guarantees that the largest eigenvalue is positive and real is provided by the Perron-Frobenius theorem, which states that there exists a positive real eigenvalue $\bar{\sigma}$ such that all other eigenvalues of the real matrix Γ satisfy $|\sigma_i| < \bar{\sigma}$, if either Γ is positive ($\gamma_{ij} > 0$ for all i, j) or Γ is non-negative and primitive. That is, $\gamma_{ij} \geq 0$ for all i, j and there exists a $k \in \mathbb{N}$ such that Γ^k is positive [30]. A different case occurs if Γ is non-negative and irreducible, but not primitive. A matrix is irreducible if the corresponding network is strongly connected, that is, there is a path from each node to every other node [30]. For this case, the Perron-Frobenius theorem states that there exist eigenvalues other than $\bar{\sigma}$ with equal magnitude (that is, $|\sigma_i| \leq \bar{\sigma}$). Equation (9) still gives the bifurcation threshold, but more than one network mode will reach the threshold (within the accuracy of our stability boundary approximation).

The coupling architecture of the experiment, where two oscillators without self-coupling are linked to one another, is an example of the latter case.

V. THE SCALING LAW OF THE OSCILLATION AMPLITUDES

We found that all experimental data for the growth of the oscillation amplitude could be collapsed onto a single curve for coupling strengths close to the bifurcation threshold.

The reason that there exists a single function relating the amplitudes to the asymmetric coupling strengths is that the network becomes unstable via an Andronov-Hopf bifurcation of the most unstable network mode, for example, the in-phase oscillation mode in our experiment. Any Andronov-Hopf bifurcation close to the bifurcation threshold can be described by the polar-coordinate normal form [29]

$$\begin{aligned}\dot{\rho} &= \mu K_1 \rho + K_2 \rho^3 + O[\mu^2 \rho + |(\mu, \rho)|^4], \\ \dot{\xi} &= -\Omega + O(|\mu, \rho|).\end{aligned}\quad (11)$$

Here, Ω is the imaginary part of the characteristic values associated with the bifurcation, K_1 and K_2 are real coefficients, and μ is the bifurcation parameter with $\mu = (\sqrt{\gamma_{12}\gamma_{21}} - \gamma_c) f'(0)$ for the cross-coupled oscillators. The qualitative behavior of the asymptotic solutions of the system equations, Eqs. (1)–(3), is the same as the behavior of solutions of Eq. (11), which, in turn, depends only on the signs of the two coefficients K_1 and K_2 . The case $K_1 > 0$ and $K_2 < 0$ corresponds to a supercritical bifurcation with an amplitude growth of the network mode given by

$$\rho(\mu) = \sqrt{-\mu \frac{K_1}{K_2}}. \quad (12)$$

Clearly the amplitude of either one of the two cross-coupled oscillators has to grow as $x_i^{\max} \propto \sqrt{\mu}$ for $\mu > 0$, in agreement with the observed behavior. This is true for any system undergoing an Andronov-Hopf bifurcation.

However, to arrive at an explicit scaling law that allows one to collapse all the data onto a single curve, one has to explicitly perform the mapping of the system equations, Eqs. (1)–(3), onto the normal form, Eq. (11). This is necessary because experimentally we measure x_1 as a function of γ_{12} for a variety of fixed values of γ_{21} , whereas the Hopf-normal form provides ρ as a function of μ . This difference enters in two ways. First, the mapping from x_1 to ρ depends on the coupling strengths and, second, the parameters K_1 and K_2 , which are determined at the bifurcation threshold, $\mu = 0$, become functions of γ_{21} .

The normal form mapping is performed using the theory developed in Refs. [31], where the formal adjoint theory for linear DDE's [28] is utilized to set up an appropriate coordinate system near an equilibrium point. One then proceeds by performing a sequence of transformations of variables such that, at each step j , the change of variables affects simultaneously the projection of the original DDE onto the center manifold and removes the nonresonant terms of order j from the ordinary differential equation ordinary differential equation on it.

Considering the linear mapping between the network modes and the original variables, we find that x_1 , corresponding to the measured voltage, is related to ρ via

$$x_1(t) = 2\sqrt{\frac{\gamma_{12}}{\gamma_{21}}} \rho \cos(\Omega t) \simeq 2\frac{\gamma_c}{\gamma_{21}} \rho \cos(\Omega t), \quad (13)$$

where we used that $\gamma_{12} = \gamma_c^2/\gamma_{21}$ at the bifurcation threshold. Going beyond the linear analysis, the Hopf bifurcation is determined generically up to third order [see Eq. (11)], which implies that the Taylor expansion of the nonlinearity up to third order is relevant. For the bias condition in the experiment, the

expansion of f in Eq. (1) about the steady state results in

$$f'(0) = d, \quad f''(0) = 0, \quad f'''(0) = -2d(1 + 2d^2).$$

Using these derivatives and carrying out the analysis, which is entirely analogous to the case of a single system as discussed in [26], we find

$$K_1 = \text{Re} \left\{ \left[e^{i\Omega\tau} \left(1 + \frac{\epsilon}{\Omega^2} \right) + \tau d \gamma_c \right]^{-1} \right\} > 0 \quad (14)$$

and

$$K_2 = -\frac{d(1 + 2d^2)\gamma_c(\gamma_{21}^2 + \gamma_c^2)}{2\gamma_{21}^2} K_1 < 0. \quad (15)$$

Combining Eqs. (12)–(15), we obtain

$$V_1^{\text{rms}} \propto x_1^{\max} \propto \frac{\sqrt{\sqrt{\gamma_{12}\gamma_{21}} - \gamma_c}}{\sqrt{\gamma_{21}^2 + \gamma_c^2}}, \quad (16)$$

providing us with the γ_{21} -dependent scaling that maps all data onto a single curve for values of the coupling strengths close to the bifurcation threshold. The predicted amplitude growth provides a good description that extends well into the parameter region where the oscillations become square-wave-like, as can be seen in Fig. 3(b).

VI. DISCUSSION

We have studied experimentally the influence of asymmetric coupling strengths on the oscillation onset in an experimental system of two cross-coupled optoelectronic oscillators with time delay. Oscillations arise through Andronov-Hopf bifurcations from steady state, if the product of the two coupling strengths exceeds a critical value. Linear stability analysis was used to show that the coupling-strength product is the relevant bifurcation parameter for any cross-coupled system and that the critical value is identical to the critical value of self-coupling for which a single system starts to oscillate.

More generally, the stability analysis of a large coupled network can be reduced to the level of complexity of one single oscillator, similar to the master stability function approach of Pecora and Carroll [32]. This reduction shows that the relation between the coupling strengths and the effective bifurcation parameter is a function of the network architecture only.

Carrying out the stability analysis for single oscillators belonging to the important class of single-input–single-output systems with long delay, we find that one generically expects an Andronov-Hopf bifurcation to occur, if the transfer function has bandpass characteristics. The class of delay systems with bandpass characteristics that are discussed here includes a number of the recently developed well-controlled laboratory systems that have been used to investigate the complex dynamics arising from the interaction of nonlinearities and delay, such as electronic oscillators with delayed feedback [27,33], optoelectronic devices with interferometric nonlinearity [18,25,34,35], and optoelectronic devices where the nonlinearity is due to the internal dynamics of semiconductor lasers [5,9,17].

Going beyond the linear stability analysis, we have made use of standard normal form theory for DDE's [29] to derive a scaling law for the amplitudes of the oscillations past the

bifurcation threshold. We find that this approach provides a surprisingly good description of the observed behavior even for coupling strengths for which the square root of their product exceeds the threshold value by 20%.

When considering other experimental systems, the precise form of the scaling law will differ from the one derived here, Eq. (16), because it depends on the nonlinearity of the system. However, a scaling law will always exist because the Hopf-normal form captures the asymptotic dynamics of any system close to the Andronov-Hopf bifurcation threshold. As an example, Kim *et al.* [9] demonstrated the existence of a scaling law for cross-coupled optoelectronic oscillators that utilize a semiconductor laser as a nonlinear element, yet the form of the scaling is different from Eq. (16).

Another point that needs to be emphasized is that the normal-form approach describes the amplitude growth of a single periodic solution branch sufficiently close to the bifurcation threshold, where the solution is small and sinusoidal. “Sufficiently close” to the instability threshold of the steady state can imply, in practice, an unobservably small parameter range. For example, very-low-frequency oscillations with periods exceeding the delay time by orders of magnitude can arise in broadband optoelectronic feedback systems [18,36] for feedback strengths very close to the Hopf-bifurcation threshold. Furthermore, secondary bifurcations of the periodic solution branches born in Andronov-Hopf bifurcations might result in quasiperiodic oscillations [5,37] or the coexistence of many stable periodic solutions [17,38].

For the experiment described here, our theory provides a useful description for a considerable parameter range because the periodic solution branch created in the supercritical Andronov-Hopf bifurcation continues to be the dominant attractor for coupling strengths well in excess of the threshold value. As a result, the scaling law only starts to fail when oscillation amplitudes are large enough such that saturation effects due to the nonlinearity result in square-wave-like solutions.

ACKNOWLEDGMENT

This work was supported by the Research Corporation for Science Advancement (Award No. 7847).

APPENDIX: LINEAR STABILITY ANALYSIS OF SINGLE-INPUT-SINGLE-OUTPUT SYSTEMS

Here we explicitly carry out the linear stability analysis for a network of single-input–single-output systems with bandpass-filter characteristics and show that one generically expects the steady state to become unstable via an Andronov-Hopf bifurcation and that the stability boundary in the complex σ parameter plane is a circle, to good approximation.

We argued that the stability of the steady state can be analyzed by investigating the set of uncoupled linear DDE’s given by Eq. (8). The corresponding characteristic equation is

$$\prod_{i=1}^N \det(\lambda \mathbb{1}_m - DF - \sigma_i \mathbf{bc} e^{-\lambda\tau}) = 0, \quad (\text{A1})$$

where we used $DH = \mathbf{bc}$. The network is stable if all characteristic values λ have a negative real part. Alternatively,

utilizing the factorization, the network is stable if all the network eigenvalues σ_i fall in the single-system stability region. To determine the boundary of this steady-state stability region, one seeks, for a single factor in Eq. (A1), solutions σ for which the characteristic value λ has zero real part, $\lambda = i\Omega$. In this analysis, σ is treated as a complex parameter and one solves for the curve in the σ parameter plane that bounds the stability region. Furthermore, it suffices to consider $\lambda = i\Omega$ with $\Omega \geq 0$ because the characteristic values associated with the entire network will cross the imaginary axis either in complex-conjugate pairs or along the real axis.

Having reduced the analysis to that of one single oscillator, we would like to discuss its steady-state stability in terms of its transfer function. To make a connection between the transfer function and the characteristic equation, let us return for a moment to the DDE model of a linearized single system with self-feedback and complex self-coupling strength σ ,

$$\dot{\mathbf{x}} = DF \mathbf{x} + \sigma \mathbf{bc} \mathbf{x}^\tau. \quad (\text{A2})$$

Here, the output is $y = \mathbf{cx}$. A linear input-output system of the form given by Eq. (A2) is observable if the observability matrix $[\mathbf{c}, \mathbf{c}DF, \mathbf{c}DF^2, \dots, \mathbf{c}DF^{m-1}]^T$ is nonsingular, that is, has a rank of m . It is then possible to determine the internal state of the system from the output time series. If the observability matrix has a rank m_O with $m_O < m$, then one can find coordinates in which the states are decomposed into m_O observable states and $m - m_O$ unobservable states. The differential equation describing the dynamics of the observable states is decoupled from that of the unobservable states and it suffices to consider the m_O -dimensional reduced-order observable state equations [39,40]. For simplicity, we presume the system given by Eq. (A2) is observable ($m_O = m$). It then can be brought, through a linear coordinate transformation $\bar{\mathbf{x}} = \mathbf{T} \mathbf{x}$, into canonical form [40],

$$\dot{\bar{\mathbf{x}}} = \overline{DF} \bar{\mathbf{x}} + \sigma \bar{\mathbf{b}} \bar{\mathbf{x}}^\tau, \quad (\text{A3})$$

with output $y = \bar{\mathbf{x}}_m$ and input $u = \sigma \bar{\mathbf{x}}_m^\tau$. Here, $\bar{\mathbf{b}}$ and \overline{DF} are given by

$$\overline{DF} = \begin{bmatrix} 0 & \cdots & 0 & -d_m \\ & & -d_{m-1} & \\ & & \vdots & \\ \mathbb{1}_{m-1} & & & -d_1 \end{bmatrix}, \quad \bar{\mathbf{b}} = \mathbf{T} \mathbf{b} = \begin{bmatrix} n_m \\ n_{m-1} \\ \vdots \\ n_1 \end{bmatrix},$$

where the d_i are the real coefficients of the polynomial

$$\det(s \mathbb{1}_m - DF) = s^m + d_1 s^{m-1} + \cdots + d_{m-1} s + d_m.$$

The strictly proper transfer-function corresponding to Eq. (A3) [and Eq. (A2)] is

$$H(s) = \frac{N(s)}{D(s)} = \frac{\sum_{j=1}^m n_j s^{m-j}}{s^m + \sum_{j=1}^m d_j s^{m-j}}.$$

We can now state what we mean by bandpass characteristics. If the magnitude of the transfer function, $|H(i\omega)|$, has a single global maximum at some nonzero frequency ω_{\max} , then H will look like a two-pole bandpass filter for frequencies close to ω_{\max} . For systems with sufficiently long delay, there will exist in the vicinity of ω_{\max} a possible oscillation mode of the system because the frequency spacing between two adjacent

modes scales as $\Delta\omega \propto \tau^{-1}$. Therefore, only the part of H around this global maximum is relevant when investigating bifurcations from the steady state for systems with long delay, and the discussions of systems with two-pole bandpass-filtered delayed feedback in [26] are applicable.

Mathematically this idea carries through as follows. The characteristic values λ that determine the stability of the steady-state solution of Eq. (A2) are the roots of a single factor in Eq. (A1), that is, the roots of

$$\chi(\lambda) = \det(\lambda \mathbb{1}_m - DF - \sigma \mathbf{bc} e^{-\lambda\tau}) = 0. \quad (\text{A4})$$

Noting that

$$\chi(\lambda) = D(\lambda) - N(\lambda)\sigma e^{-\lambda\tau} \quad (\text{A5})$$

and using the notation

$$\sigma = |\sigma|e^{i\Psi}$$

for the complex self-coupling strength, one finds that the characteristic values λ are solutions to

$$1 = H(\lambda) |\sigma| e^{i\Psi} e^{-\lambda\tau}. \quad (\text{A6})$$

Using the ansatz $\lambda = i\Omega = i\omega_{\max} + i\Delta$ and expanding the transfer function $H(i\Omega) = |H(i\Omega)| \exp[i\Phi(\Omega)]$ in the vicinity of its global maximum to lowest order in Δ gives

$$H \approx [|H(i\omega_{\max})| - O(\Delta^2)] e^{-i(\tau_\phi\omega_{\max} + \tau_g\Delta)}, \quad (\text{A7})$$

where $\tau_\phi = -\Phi(\omega)/\omega|_{\omega_{\max}}$ and $\tau_g = -d\Phi(\omega)/d\omega|_{\omega_{\max}}$ are the phase and group delay, respectively. Using Eq. (A7) in

Eq. (A6) and matching the phases results in an equation for Δ ,

$$(\tau_g + \tau)\Delta = -\tau_\phi\omega_{\max} - \omega_{\max}\tau + \Psi - 2\pi n. \quad (\text{A8})$$

Generically, there will be one mode that destabilizes the steady state. This mode corresponds to the integer mode number n that minimizes the magnitude of the right-hand side of Eq. (A8), yielding the estimate

$$|\Delta| \lesssim \frac{\pi}{|\tau_g + \tau|}. \quad (\text{A9})$$

The above estimate shows that $|\Delta| \propto \tau^{-1}$ as long as $\tau \gg |\tau_g|$ holds. This demonstrates that our approximation is useful and the mode frequency is close to ω_{\max} in the limit of long delays ($\omega_{\max}\tau \gg 1$). In this limit, the critical gain is

$$|\sigma|_c = |H(i\omega_{\max})|^{-1} + O(\tau^{-2}). \quad (\text{A10})$$

In other words, the stability boundary in the complex σ parameter plane approaches a circle as the delay increases, the deviation being of order τ^{-2} . Therefore, for systems with large delay, the least stable oscillatory mode of a network will start to grow when the magnitude of the corresponding eigenvalue will reach the value of the critical coupling strength of a single system, $|\sigma_i| \simeq \gamma_c$. Furthermore, the bandpass characteristics of the transfer function guarantees that generically the steady state loses stability via an Andronov-Hopf bifurcation. The exceptions are special values of the delay, where two pairs of characteristic values cross simultaneously the imaginary axis and a double-Hopf bifurcation occurs.

-
- [1] S. H. Strogatz, *Nature (London)* **410**, 268 (2001).
 [2] V. K. Jirsa and M. Ding, *Phys. Rev. Lett.* **93**, 070602 (2004).
 [3] C. Masoller, M. C. Torrent, and J. Garca-Ojalvo, *Phys. Rev. E* **78**, 041907 (2008).
 [4] N. A. Cookson, L. S. Tsimring, and J. Hasty, *FEBS Lett.* **583**, 3931 (2009).
 [5] H. D. I. Abarbanel, M. B. Kennel, L. Illing, S. Tang, H. F. Chen, and J. M. Liu, *IEEE J. Quantum Electron.* **37**, 1301 (2001).
 [6] T. Heil, I. Fischer, W. Elsasser, J. Mulet, and C. R. Mirasso, *Phys. Rev. Lett.* **86**, 795 (2001).
 [7] J. Mulet, C. Mirasso, T. Heil, and I. Fischer, *J. Opt. B* **6**, 97 (2004).
 [8] M. C. Chiang, H. F. Chen, and J. M. Liu, *IEEE J. Quantum Electron.* **41**, 1333 (2005).
 [9] M. Y. Kim, R. Roy, J. L. Aron, T. W. Carr, and I. B. Schwartz, *Phys. Rev. Lett.* **94**, 088101 (2005).
 [10] T. W. Carr, I. B. Schwartz, M. Y. Kim, and R. Roy, *SIAM J. Appl. Dyn. Syst.* **5**, 699 (2006).
 [11] I. Fischer, R. Vicente, J. M. Buldu, M. Peil, C. R. Mirasso, M. C. Torrent, and J. Garcia-Ojalvo, *Phys. Rev. Lett.* **97**, 123902 (2006).
 [12] E. A. Rogers-Dakin, J. Garcia-Ojalvo, D. J. DeShazer, and R. Roy, *Phys. Rev. E* **73**, 045201 (2006).
 [13] M. Peil, L. Larger, and I. Fischer, *Phys. Rev. E* **76**, 045201 (2007).
 [14] I. Kanter, N. Gross, E. Klein, E. Kopelowitz, P. Yoskovits, L. Khaykovich, W. Kinzel, and M. Rosenbluh, *Phys. Rev. Lett.* **98**, 154101 (2007).
 [15] I. B. Schwartz and L. B. Shaw, *Phys. Rev. E* **75**, 046207 (2007).
 [16] F. T. Arecchi, G. Giacomelli, A. Lapucci, and R. Meucci, *Phys. Rev. A* **43**, 4997 (1991).
 [17] G. Giacomelli and A. Politi, *Physica D* **117**, 26 (1998).
 [18] M. Peil, M. Jacquot, Y. K. Chembo, L. Larger, and T. Erneux, *Phys. Rev. E* **79**, 026208 (2009).
 [19] K. E. Callan, L. Illing, Z. Gao, D. J. Gauthier, and E. Scholl, *Phys. Rev. Lett.* **104**, 113901 (2010).
 [20] O. D’Huys, R. Vicente, T. Erneux, J. Danckaert, and I. Fischer, *Chaos* **18**, 037116 (2008).
 [21] O. D’Huys, R. Vicente, J. Danckaert, and I. Fischer, *Chaos* **20**, 043127 (2010).
 [22] W. Kinzel, A. Englert, G. Reents, M. Zigzag, and I. Kanter, *Phys. Rev. E* **79**, 056207 (2009).
 [23] V. Flunkert, S. Yanchuk, T. Dahms, and E. Scholl, *Phys. Rev. Lett.* **105**, 254101 (2010).
 [24] L. B. Shaw, I. B. Schwartz, E. A. Rogers, and R. Roy, *Chaos* **16**, 015111 (2006).
 [25] T. E. Murphy, A. B. Cohen, B. Ravoori, K. R. B. Schmitt, A. V. Setty, F. Sorrentino, C. R. S. Williams, E. Ott, and R. Roy, *Philos. Trans. R. Soc. London, Ser. A* **368**, 343 (2010).
 [26] L. Illing and D. J. Gauthier, *Physica D* **210**, 180 (2005).
 [27] L. Illing and D. J. Gauthier, *Chaos* **16**, 033119 (2006).

- [28] J. K. Hale and S. M. V. Lunel, *Introduction to Functional Differential Equations* (Springer-Verlag, New York, 1993).
- [29] J. Hale, L. T. Magalhães, and W. L. Oliva, *Dynamics in Infinite Dimensions* (Springer, New York, 2002).
- [30] A. Berman and R. J. Plemmons, *Nonnegative Matrices in the Mathematical Sciences* (Society for Industrial and Applied Mathematics, Philadelphia, 1994).
- [31] T. Faria and L. T. Magalhães, *J. Differential Equations* **122**, 181 (1995); **122**, 201 (1995).
- [32] L. M. Pecora and T. L. Carroll, *Phys. Rev. Lett.* **80**, 2109 (1998).
- [33] V. S. Udaltsov, L. Larger, J. P. Goedgebuer, M. W. Lee, E. Genin, and W. T. Rhodes, *IEEE T. Circ. I* **49**, 1006 (2002).
- [34] J. P. Goedgebuer, P. Levy, L. Larger, C. C. Chen, and W. T. Rhodes, *IEEE J. Quantum Electron.* **38**, 1178 (2002).
- [35] J. N. Blakely, L. Illing, and D. J. Gauthier, *IEEE J. Quantum Electron.* **40**, 299 (2004).
- [36] Y. C. Kouomou, P. Colet, L. Larger, and N. Gastaud, *Phys. Rev. Lett.* **95**, 203903 (2005).
- [37] R. Vicente, S. Tang, J. Mulet, C. R. Mirasso, and J.-M. Liu, *Phys. Rev. E* **70**, 046216 (2004).
- [38] M. Wolfrum and S. Yanchuk, *Phys. Rev. Lett.* **96**, 220201 (2006).
- [39] R. E. Kalman, *Proc. Natl. Acad. Sci. USA* **48**, 596 (1962).
- [40] M. Gopal, *Modern Control System Theory*, 2nd ed. (Wiley, New York, 1993).